Effect of carbon content and annealing on structure and hardness of $CrFe_2NiMnV_{0.25}$ high entropy alloys processed by high-pressure torsion

Hamed Shahmir[a,b,*], Elena Tabachnikova[c], Aleksey Podolskiy[c],
Mikhail Tikhonovsky[d], Terence G. Langdon[a],

[a] *Materials Research Group, Faculty of Engineering and the Environment, University of Southampton, Southampton SO17 1BJ, UK*
[b] *School of Metallurgy and Materials, College of Engineering, University of Tehran, Tehran, Iran*
[c] *B. Verkin Institute for Low Temperature Physics and Engineering of National Academy of Sciences of Ukraine, 47 Nauky Ave., Kharkov, 61103, Ukraine*
[d] *National Science Center «Kharkov Institute of Physics and Technology» of National Academy of Sciences of Ukraine, 1 Academicheskaya Street, Kharkov, 61108, Ukraine*

Abstract

$CrFe_2NiMnV_{0.25}C_{0.075}$ and $CrFe_2NiMnV_{0.25}C_{0.125}$ high entropy alloys (HEA) were processed by high-pressure torsion (HPT) followed by post-deformation annealing (PDA) at 823 and 1273 K. This severe plastic deformation led to a significant microhardness increment (by a factor of ~2.5) up to ~435 Hv and the microstructures exhibited exceptional grain refinement with average grain sizes of ~30 nm in both HEAs. It was found that the hardness increased up to ~555 Hv after annealing at 823 K due to precipitation of the σ phase but thereafter the hardness decreased to ~195 Hv after annealing at 1273 K which was very close to the value of the initial coarse-grained condition. This behavior is caused by a combination of grain coarsening and a dissolution of the precipitates. These results suggest that the nanocrystalline HEA facilitates the formation of precipitates owing to the large number of grain boundaries which serve both as fast diffusion pathways and as preferential nucleation sites for precipitate formation.

Keywords: $CrFe_2NiMnV_{0.25}$; High-entropy alloy; High-pressure torsion; Post deformation annealing; Severe plastic deformation.

[*]Corresponding author. Tel.: +982182084163
E-mail address: h.shahmir@ut.ac.ir

Introduction

Equiatomic or near-equiatomic high entropy alloys (HEAs) have attracted much attention due to their potential beneficial mechanical characteristics, such as high strength, high fracture toughness, good ductility and good wear resistance [1]. In addition, some HEAs contain five or more elements, with the concentration of each element between 5 and 35 at.%, and these alloys have high configurational entropy such that $S_{mix}>1.61R$ where R is the gas constant. This serves to suppress the formation of an intermetallic phase and may favor the formation of simple *fcc* or *bcc* structures based on solid solution phases [2,3].

In order to increase the strength of these alloys without significantly sacrificing their ductility, additional strengthening methods may be introduced such as solid solution or precipitation hardening which requires thermomechanical processing or modifications of the chemical compositions of the alloys [4-7]. It is well known that, in addition to the principal elements, HEAs may also contain minor elements with each below 5 at.% [8]. Improvements in the mechanical properties of metallic alloys are traditionally achieved by doping [9] and doping elements such as carbon, for the formation of high-strength fine carbides, may lead to improvements in the strength of HEAs. In addition, it is reasonable to anticipate that the additional strengthening method of grain refinement, achieved through processing by severe plastic deformation (SPD), may lead to improvements in the mechanical properties of HEAs. Equal-channel angular pressing (ECAP) [10] and high-pressure torsion (HPT) [11] are well-established SPD procedures for achieving ultrafine and even nanostructured grains in metals and alloys but HPT is generally advantageous because, by comparison with ECAP, it produces smaller grain sizes [12,13] and higher fractions of grain boundaries having high angles of misorientation [14].

Several reports are now available describing the influence of HPT processing on HEAs [15-24] and there is also a single report documenting the processing of an HEA by ECAP [25]. It was shown earlier that processing a CoCrFeNiMn high-entropy alloy by HPT leads to significant hardening and grain refinement and, in addition, post-deformation annealing (PDA) of the nanocrystalline CoCrFeNiMn HEA provides an excellent combination of high strength and good ductility [19]. Experiments also showed that a nanocrystalline CoCrFeNiMn HEA processed by HPT exhibited excellent ductility at elevated temperatures including superplastic elongations with a maximum elongation of >600% at a testing temperature of 973 K [22,26].

One of the potential methods for increasing the strength of HEAs with an *fcc* crystal lattice is doping by carbon for the formation of high-strength fine carbides. Nevertheless, the influence of these carbides on the structure and properties of HEAs has received only limited attention. Accordingly, the present research was initiated to evaluate the effect of grain refinement due to HPT on the microstructures of two different $CrFe_2NiMnV_{0.25}$ HEAs doped by carbon.

Experimental materials and procedures

$CrFe_2NiMnV_{0.25}C_{0.075}$ and $CrFe_2NiMnV_{0.25}C_{0.125}$ high entropy alloys were prepared using a non-consumable vacuum arc melting technique in a water-cooled copper crucible. The purities of the alloying elements were above 99.9 at.%. After several remeltings (5 times) for homogenization, the ingots were hot forged and homogenized at 1323 K for 1 h. Then the samples were cold-rolled to ~30 % thickness reduction followed by annealing at 1373 K for 1 h. To prevent oxidation, all samples were sealed in vacuum quartz tubes filled with titanium chips before the heat treatments. Polished disks with diameters of 10 mm and thicknesses of ~0.8 mm were prepared from the initial annealed alloys and then processed by HPT for 5 turns at room temperature (RT) under an applied pressure of 6.0 GPa at 1 rpm using quasi-constrained conditions in which there is a small outflow of material around the peripheries of the disks

during the torsional straining [27]. The disks subjected to HPT through 5 rotations were used for post deformation annealing (PDA) at 823 and 1273 K for 60 min. In addition, similar heat treatment was conducted for the initial annealed samples.

Following the processing operation, these disks were polished in order to achieve a mirror-like quality and then hardness measurements were recorded using a Vickers microhardness tester. Each reading was taken using a load of 500 gf and an indentation dwell time of 10 s. The average microhardness values, Hv, were recorded along diameters selected randomly with the measurements taken at intervals of ~0.5 mm. At each of these points the local value of Hv was obtained by averaging four separate hardness values.

The phase constituents were determined from X-ray diffraction (XRD) using Rigaku SmartLab equipment with Cu Kα radiation having a wavelength, λ, of 0.154 nm at 45 kV and with a tube current of 200 mA. All XRD measurements were conducted over angular ranges of 2θ from 30° to 100° with a scanning step of 0.01° and a speed of scanning of $2^{o}\ min^{-1}$.

The microstructures were characterized using optical microscopy (OM), scanning electron microscopy (SEM) and transmission electron microscopy (TEM). SEM investigations were performed using a JEOL JSM-7001F 00 microscope equipped with Energy dispersive X-ray spectroscopy (EDS). For TEM, the foils were prepared both before PDA and after PDA at a temperature of 823 K for 60 min. This was accomplished using a focused ion beam (FIB) Zeiss Nvision 40 FIB facility at a distance of 3 mm from the $CrFe_2NiMnV_{0.25}C_{0.125}$ HEA disk centres in the normal sections of the disks. This means that the normals of the images are lying in the shear direction. All of the TEM micrographs were recorded using a JEOL JEM-3010 microscope which was operated with an accelerating voltage of 300 kV.

Experimental results

Initial microstructure of HEA

Figure 1 shows the microstructure of $CrFe_2NiMnV_{0.25}C_{0.125}$ HEA in as-cast state (a,b) and after cold-rolling and annealing at 1373 K for 1 h (c,d) investigated by OM and SEM, respectively. The observations reveal an extended dendritic structure in Fig. 1(a) including lighter dendrites and darker interdendritic areas as shown in the higher magnification image in Fig. 1(b). The size of dendritic branches is up to several hundred micrometers. Interdendritic areas are two-phase eutectic microstructure consisting of matrix and carbide phases as was shown earlier for the alloy $CrFe_2NiMnV_{0.25}C_{0.175}$ [28]. The microstructure of the $CrFe_2NiMnV_{0.25}C_{0.075}$ HEA revealed similar regularities but the volume fraction of carbides was slightly lower (not shown). The annealed sample after cold-rolling shows a coarse-grained microstructure represented in Fig. 1 (c,d) with a grain size of ~10-40 μm with carbides distributed in the matrix. Close inspection of Fig. 1 (d) reveals that the size of carbides is ~1 μm and some of them have been detached from the matrix due to their weak interfaces with the matrix during sample preparation for microstructural investigations. A comparison of the carbide size in as-cast and after cold-rolling followed by annealing indicates the crushing of carbides during hot forging and cold-rolling.

Chemical analyses of the matrix and carbides in $CrFe_2NiMnV_{0.25}C_{0.125}$ HEA before HPT processing were investigated using EDS and the results are summarized in Table 1. The nominal and experimental compositions of the HEA are reported in this Table as well. It is important to note that the carbon concentration is not shown due to the limited sensitivity used in the experimental system to light elements. The results indicate that the matrix phase is substantially depleted of chromium and vanadium and the carbide particle consists mainly of chromium and also the amount of vanadium is significant in comparison to the matrix.

Hardness evaluations before and after HPT processing

Figure 2 shows the results for the Vickers microhardness measurements after processing through 5 turns. The average values of Hv are plotted along each disk diameter and in Fig. 2

the lower dashed lines at Hv ≈ 170 and 180 correspond to the initial hardness in the initial coarse- grained $CrFe_2NiMnV_{0.25}C_{0.075}$ and $CrFe_2NiMnV_{0.25}C_{0.125}$ HEAs, respectively. The results show clearly that there is a significant increase in hardness at the edge of the disk after 5 turns with incremental increases by factors of ~2.5 to Hv ≈ 430 and ~435 with respect to the annealed condition for the $CrFe_2NiMnV_{0.25}C_{0.075}$ and $CrFe_2NiMnV_{0.25}C_{0.125}$ HEAs, respectively. These results demonstrate that after 5 turns it is not possible to produce a fully-homogeneous hardness distribution. On the contrary, the results show there is a very small area around the centres of the disks, within a radius of r < 1 mm, where the hardness values are significantly lower (Hv ≈ 350) in both HEAs. The results demonstrate also there is no significant difference between the hardness of samples processed by HPT through 5 turns at radii which are larger than ~1 mm.

Microstructures before and after HPT processing

XRD patterns for both the initial annealed samples (not processed by HPT) and near the edges of disks after HPT through totals of N = 5 turns for $CrFe_2NiMnV_{0.25}C_{0.075}$ and $CrFe_2NiMnV_{0.25}C_{0.125}$ are shown in Fig. 3(a) and Fig. 3(b), respectively. Inspection of the patterns reveals that the annealed microstructures consist of an *fcc* phase marked with solid circles and peaks marked with solid inverted triangles with the main peak at 2θ ≈ 43.9º related to the $Cr_{23}C_6$-like phase. It was previously shown [28] that in the Cr-Fe-Ni-Mn-V-C HEAs the carbide phase has the structure of Cr_7C_3 compound in the as-cast state but it transforms into $Cr_{23}C_6$ phase on annealing below 1473 K [30]. The volume fraction of the secondary phase of chromium carbide in the initial coarse-grained state was ~7% as determined by X-ray diffraction analysis. The patterns reveal also that HPT processing causes a peak broadening in the HEAs but there is no evidence for the creation of any new phases or the occurrence of any phase transformations as a results of the HPT processing.

The microstructure of the $CrFe_2NiMnV_{0.25}C_{0.125}$ HEA is shown in Fig. 4 after 5 turns of HPT at a position near the edge areas without any particles in Fig. 4(a) and with a chromium carbide particle in Fig. 4(b). Inspection shows that the processed microstructure consists primarily of an array of equiaxed nanostructured grains that have an average size of ~30 nm but with many of the grains surrounded by grain boundaries that are diffuse or ill-defined as in Fig. 4(a). In addition, there is visible strain contrast in many of these grains and this is generally associated with the presence of dislocations. The appearance of this microstructure is typical of other materials prepared using different SPD techniques and it demonstrates the presence of a significantly large volume of high-energy non-equilibrium boundaries [29].

The microstructure contains an *fcc* phase in this area with boundaries having high angles of misorientation and this is apparent from the arrangement of the diffraction spots in semi-continuous circles in the selected area electron diffraction (SAED) pattern as shown by the inset in Fig. 4(a). A particle surrounded by matrix grains is shown in Fig. 4(b) and energy dispersive X-ray spectroscopy (EDS) of the two regions marked A and B confirmed from the chemical compositions that these neighbouring areas were different phases. Specifically, the chemical composition of region A corresponded to the composition of the HEA matrix and the composition of region B corresponded to chromium carbide which is consistent with the XRD results. A comparison between the particle sizes before HPT (several microns) and after HPT processing (<1 μm) confirmed that the particles were crushed due to the high shear stresses imposed in the HPT processing.

Microstructures after post-deformation annealing

Figure 5 uses XRD to demonstrate the microstructural evolution in the $CrFe_2NiMnV_{0.25}C_{0.125}$ samples after annealing at 823 and 1273 K for 60 min. The effect of this subsequent annealing on the initial annealed microstructure is shown in Fig. 5(a) and the effect on the HPT-processed material is shown in Fig. 5(b). Inspection reveals the appearance of some additional peaks of

very low intensities marked with open inverted triangles in the samples annealed at 823 K in both the initial annealed and the HPT-processed samples. The crystal structure of this new phase may be identified as tetragonal and the lattice parameters are given by $a \approx 8.8$ Å and $c \approx 4.5$ Å. This corresponds to the σ-phase which is a hard Cr-rich phase reported earlier in some HEAs processed by SPD [16-22,24]. These XRD results indicate that the volume fraction of the σ-phase was ~3% and ~6% in the annealed and HPT-processed samples, respectively, and close inspection shows an absence of this phase after annealing at 1273 K.

A scanning transmission electron microscopy (STEM) image is shown in Fig. 6 for a $CrFe_2NiMnV_{0.25}C_{0.125}$ sample after HPT for 5 turns followed by PDA at 823 K for 60 min. Thus, in this condition the microstructure contains essentially equiaxed grains with an estimated mean grain size of ~200 nm. There are some small darker phases in the STEM micrograph and, according to the corresponding XRD results (Fig. 5b), these phases appear to be Cr-rich precipitates. It is apparent also that this Cr-rich phase is distributed reasonably homogenously throughout the microstructure in Fig. 6 with an average size of ~100 nm.

Table 2 records the measured values of the microhardness for the initial coarse-grained $CrFe_2NiMnV_{0.25}C_{0.125}$ HEA and for the HPT-processed samples both in their initial conditions and after annealing at temperatures of 823 and 1273 K for a period of 60 min. The results demonstrate also that the hardness of the nanocrystalline HEA increases slightly up to Hv ≈ 555 after annealing at 823 K but thereafter it decreases after annealing at 1273 K. At this temperature the measured hardness is ≈195 which is close to the value of Hv ≈ 180 for the initial coarse-grained condition. It is interesting to note that there is a similar trend in the initial annealed sample but with a maximum hardness of only Hv ≈ 190 after annealing at 823 K. This suggests that the precipitates form at 823 K in both conditions and it is important to note this is consistent with the XRD results as shown in Fig. 5.

Discussion

Effect of HPT and carbon content on the microstructures of HEAs

The XRD and hardness results show that there is no significant difference between the $CrFe_2NiMnV_{0.25}C_{0.075}$ and $CrFe_2NiMnV_{0.25}C_{0.125}$ HEAs after HPT processing. The hardness of $CrFe_2NiMnV_{0.25}C_{0.125}$ is marginally larger than $CrFe_2NiMnV_{0.25}C_{0.075}$ with a lower carbon content but the volume fractions of chromium carbide are almost the same at ~7% in both HEAs. The microstructural observations of the $CrFe_2NiMnV_{0.25}C_{0.125}$ HEA after HPT processing reveal exceptional grain refinement to ~30 nm with a dispersion of chromium carbide nanoparticles within the *fcc* matrix. It has been shown that grain refinement in the single-phase HPT-processed CoCrFeNiMn alloy is more efficient with grain sizes of ~10 nm [19] by comparison with the $CrFe_2NiMnV_{0.25}C_{0.125}$ HEA. Thus, the presence of carbides in the $CrFe_2NiMnV_{0.25}C_{0.125}$ HEA produces barriers that appear to restrict further grain refinement [30,31].

Microstructural evolution of the *fcc* HEA was studied earlier [5,32] and it was found that the most significant plasticity mechanism at low homologous temperatures was gliding of full <110> dislocations on the primary {111} planes with part of the <110> dislocations splitting into 1/6<112> Shockley partials containing stacking faults. Hard precipitates in the *fcc* HEAs, such as particles of the σ-phase, act as strong barriers for dislocation motion so that most plasticity takes place in the matrix *fcc* phase [33]. The mechanisms of plasticity in *fcc* nanocrystalline materials are not fully understood at the present time but generally it is considered that grain boundary sliding is especially important at grain sizes below ~10-15 nm whereas for larger grains the motion of partial dislocations becomes dominant and this changes to the gliding of full dislocations when the grain size increases above ~100 nm [34]. Below ~100-200 nm the plasticity is controlled by the nucleation and annihilation of dislocations at grain boundaries. At present no specific information is available on the plasticity mechanisms in nanocrystalline *fcc* HEAs but it is suggested that probably their behaviour is similar to the

mechanisms in conventional *fcc* nanocrystalline alloys. Accordingly, for HPT-processed nanocrystalline $CrFe_2NiMnV_{0.25}C_{0.075}$ and $CrFe_2NiMnV_{0.25}C_{0.125}$ HEAs with average grain sizes of ~30 nm it is reasonable to anticipate that the splitting of dislocations into partials plays an important role by comparison with their coarse-grained counterparts.

If the strength of the nanocrystalline materials is controlled by the nucleation of dislocations at grain boundaries which depends directly on the grain size, then the other contributions to yield strength typical for coarse-grained materials, such as hard particles of second phases and interstitial impurities [35], should be less important in the nanocrystalline state. Such behaviour can be observed by comparing the hardening by carbides in the $CrFe_2NiMnV_{0.25}C_{0.075}$ and $CrFe_2NiMnV_{0.25}C_{0.125}$ HEAs in Fig. 2 with earlier reports for the single phase CoCrFeNiMn HEA [16,19]. In the coarse-grained state the hardening by carbides leads to higher strength and higher hardness for $CrFe_2NiMnV_{0.25}C_{0.125}$ by comparison with CoCrFeNiMn while in the nanocrystalline state the single phase CoCrFeNiMn HEA has a higher hardness of ~450 Hv due to the smaller grain size of ~10 nm [19] compared with an average grain size of ~30 nm and a hardness of ~435 Hv in the $CrFe_2NiMnV_{0.25}C_{0.125}$ HEA. It is concluded, therefore, that hardening by carbides in the $CrFe_2NiMnV_{0.25}C_{0.125}$ HEA is less effective than hardening through the smaller grain size in the CoCrFeNiMn HEA.

Thermal stability of HEAs after PDA

The microstructures of the two HEAs consist of an *fcc* phase and chromium carbide particles before and after HPT processing but further annealing at 823 K leads to the formation of new precipitates. This is consistent with the substantial increase in hardness upon annealing and with the XRD results. The formation of precipitates in a single phase HEA after annealing within special temperature ranges is a well-known phenomenon [36-39]. For example, it was shown that the CoCrFeMnNi alloy has a single-phase *fcc* structure above 873 K but a mixture of *fcc* and *bcc* phases, or under some conditions a σ phase with a tetragonal crystal structure,

below 873 K [19]. In addition, $CoCrFeNiMnC_x$ (x = 0.1, 0.175, 0.25) HEAs demonstrate a significant increase in hardness after annealing in the temperature range of 875-1275 K due to the formation of precipitates [30,31]. The present results confirm the formation of a multi-phase nanostructured HEA after PDA at 823 K consisting of precipitates distributed within the microstructure.

Close inspection of the XRD results (Fig. 5) reveals the σ phase in the initial annealed and HPT-processed samples after annealing at 823 K. Nevertheless, these results indicate that the volume fraction of precipitates in the HPT-processed sample is higher than in the initial annealed sample. Basically, it is well known that HEAs have sluggish diffusion which affects diffusion controlled mechanisms such as precipitation and grain coarsening [40-42]. It appears that the large number of grain boundaries and imposed defects in the nanocrystalline HPT-processed alloy promote fast diffusion pathways and these pathways may act as preferential nucleation sites for the subsequent formation of precipitates. Thus, it is concluded that the severe plastic deformation produces more quickly the formation of stable precipitates by comparison with fully annealed samples.

Inspection of the hardness results in Table 2 shows the hardness decreases significantly after annealing above 823 K and up to 1273 K and this is due to the dissolution of the precipitates and the activation of grain coarsening. Thus, the final hardness at 1273 K is almost the same as in the initial annealed condition due to this coarsening. This means that the dissolution of the precipitates plays an important role in the stability of the microstructure and in the grain coarsening during annealing at 823 K.

Summary and conclusions

1. $CrFe_2NiMnV_{0.25}C_{0.075}$ and $CrFe_2NiMnV_{0.25}C_{0.125}$ high entropy alloys were processed by HPT under 6.0 GPa pressure for up to 5 turns at room temperature. After processing, the

average grain size in both HEAs was reduced to <100 nm and this grain refinement was accompanied by a significant increase in hardness.

2. The results show essentially no difference in microstructure between the $CrFe_2NiMnV_{0.25}C_{0.075}$ and $CrFe_2NiMnV_{0.25}C_{0.125}$ HEAs after HPT processing but the hardness of $CrFe_2NiMnV_{0.25}C_{0.125}$ is marginally higher than for $CrFe_2NiMnV_{0.25}C_{0.075}$ with a lower carbon content. The volume fraction of chromium carbide was almost the same at ~7% in both HEAs. Microstructural observations of the $CrFe_2NiMnV_{0.25}C_{0.125}$ HEA after HPT processing revealed exceptional grain refinement with a dispersion of very fine crushed chromium carbide particles within an *fcc* matrix.

3. The hardness of the HEA further increased after post-deformation annealing at temperatures up to 823 K due to the formation of new precipitates of the σ phase. Thereafter, the hardness decreased after annealing at even higher temperatures up to 1273 K due to grain coarsening and precipitate dissolution.

Acknowledgements

HS and TGL were supported in part by the European Research Council under Grant Agreement No. 267464-SPDMETALS.

References

1. Cantor B, Chang ITH, Knight P, Vincent AJB (2004) Microstructural development in equiatomic multicomponent alloys, Mater Sci Eng A 375-377:213-218.
2. Yeh JW, Chen SK, Lin SJ, Gan JY, Chin TS, Shun TT, Tsau CH, Chang SY (2004) Nanostructured high-entropy alloys with multiple principal elements: novel alloy design concepts and outcomes, Adv Eng Mater 6:299-303.
3. Tong CJ, Chen YL, Chen SK, Yeh JW, Shun TT, Tsau CH, Lin SJ, Chang SY (2005) Microstructure characterization of Al_xCoCrCuFeNi high-entropy alloy system with multiprincipal elements, Metall Mater Trans A 36A:881-893.
4. Otto F, Yang Y, Bei H, George EP (2013) Relative effects of enthalpy and entropy on the phase stability of equiatomic high-entropy alloys, Acta Mater 61:2628-2638.
5. Otto F, Dlouhý A, Somsen Ch, Bei H, Eggeler G, George EP (2013) The influences of temperature and microstructure on the tensile properties of a CoCrFeMnNi high-entropy alloy, Acta Mater 61:5743-5755.
6. Wang Z, Gao MC, Ma SG, Yang HJ, Wang ZH, Ziomek-Moroz M, Qiao JW (2015) Effect of cold rolling on the microstructure and mechanical properties of Al0.25CoCrFe1.25Ni1.25 high-entropy alloy, Mater Sci Eng A 645:163-169.
7. He JY, Wang H, Huang HL, Xu XD, Chen MW, Wu Y, Liu XJ, Nieh TG, An K, Lu ZP (2016) A precipitation-hardened high-entropy alloy with outstanding tensile properties, Acta Mater 102:187-196.
8. Tsai MH, Yeh JW (2014) High-entropy alloys: A critical review, Mater Res Lett 2:107-123.
9. De Boer FR (1988) In *Cohesion in Metals: Transition Metal Alloys* (Eds F.R. de Boer, D.G. Pettifor): Elsevier, New York.
10. Valiev RZ, Langdon TG (2006) Principles of equal-channel angular pressing as a processing tool for grain refinement, Prog Mater Sci 51:881-981.

11. Zhilyaev AP, Langdon TG (2008) Using high-pressure torsion for metal processing: Fundamentals and applications, Prog Mater Sci 53:893-979.

12. Zhilyaev AP, Kim B-K, Nurislamova GV, Baró MD, Szpunar JA, Langdon TG (2002) Orientation imaging microscopy of ultrafine-grained nickel, Scripta Mater 46:575-580.

13. Zhilyaev AP, Nurislamova GV, Kim B-K, Baró MD, Szpunar JA, Langdon TG (2003) Experimental parameters influencing grain refinement and microstructural evolution during high-pressure torsion, Acta Mater 51:753-765.

14. Wongsa-Ngam J, Kawasaki M, Langdon TG (2013) A comparison of microstructures and mechanical properties in a Cu–Zr alloy processed using different SPD techniques, J Mater Sci 48:4653-4660.

15. Tang QH, Huang Y, Huang YY, Liao XZ, Langdon TG, Dai PQ (2015) Hardening of an Al0.3CoCrFeNi high entropy alloy via high-pressure torsion and thermal annealing, Mater Lett 151:126-129.

16. Schuh B, Mendez-Martin F, Völker B, George EP, Clemens H, Pippan R, Hohenwarter A (2015) Mechanical properties, microstructure and thermal stability of a nanocrystalline CoCrFeMnNi high-entropy alloy after severe plastic deformation, Acta Mater 96:258-268.

17. Lee D-H, Choi I-C, Seok M-Y, He J, Lu Z, Suh J-Y, Kawasaki M, Langdon TG, Jang J-I (2015) Nanomechanical behavior and structural stability of a nanocrystalline CoCrFeNiMn high-entropy alloy processed by high-pressure torsion, J Mater Res 30:2804-2815.

18. Yu PF, Cheng H, Zhang LJ, Zhang H, Jing Q, Ma MZ, Liaw PK, Li G, Liu RP (2016) Effects of high pressure torsion on microstructures and properties of an Al0.1CoCrFeNi high-entropy alloy, Mater Sci Eng A 655:283-291.

19. Shahmir H, He JY, Lu ZP, Kawasaki M, Langdon TG (2016) Effect of annealing on mechanical properties of a nanocrystalline CoCrFeNiMn high-entropy alloy processed by high-pressure torsion, Mater Sci Eng A676:294-303.

20. Tang QH, Huang Y, Cheng H, Liao XZ, Langdon TG, Dai PQ (2016) The effect of grain size on the annealing-induced phase transformation in an Al0.3CoCrFeNi high entropy alloy, Mater Design 105:381-385.
21. Lee D-H, Seok M-Y, Zhao Y, Choi I-C, He J, Lu Z, Suh J-Y, Ramamurty U, Kawasaki M, Langdon TG, Jang J-I (2016) Spherical nanoindentation creep behavior of nanocrystalline and coarse-grained CoCrFeMnNi high-entropy alloys, Acta Mater 109:314-322.
22. Shahmir H, He JY, Lu ZP, Kawasaki M, Langdon TG (2017) Evidence for superplasticity in a CoCrFeNiMn high-entropy alloy processed by high-pressure torsion, Mater Sci Eng A685:342-348.
23. Lee D-H., Lee J-A, Zhao Y, Lu Z, Suh J-Y, Kim J-Y, Ramamurty U, Kawasaki M, Langdon TG, Jang J-I (2017) Annealing effect on plastic flow in nanocrystalline CoCrFeMnNi high-entropy alloy: A nanomechanical analysis, Acta Mater 140:443-451.
24. Shahmir H, Nili-Ahmadabadi M, Shafie A, Langdon TG (2017) Hardening and thermal stability of a nanocrystalline CoCrFeNiMnTi0.1 high-entropy alloy processed by high-pressure torsion, IOP Conf Series: Mater Sci Eng 194:012017.
25. Shahmir H, Mousavi T, He J, Lu Z, Kawasaki M, Langdon TG (2017) Microstructure and properties of a CoCrFeNiMn high-entropy alloy processed by equal-channel angular pressing, Mater Sci Eng A705:411-419.
26. Shahmir H, Kawasaki M, Langdon TG (2017) The potential for achieving superplasticity in high-entropy alloys processed by severe plastic deformation, IOP Conf Series: Mater Sci Eng 194:012040.
27. Figueiredo RB, Cetlin PR, Langdon TG (2011) Using finite element modeling to examine the flow processes in quasi-constrained high-pressure torsion, Mater Sci Eng A528:8198-8204.

28. Tikhonovsky MA, Tortika AS, Kolodiy IV, Stoev PI, Rudycheva TY, Berezhnaya NS, Tantsjura IG (2016) Microstructure and properties of high entropy alloys $CoCrFeMnNiV_{0.25}C_{0.175}$ and $CrFe2MnNiV_{0.25}C_{0.175}$, Probl Atom Sci Tech 4(104):37-41.
29. Wang J, Horita Z, Furukawa M, Nemoto M, Tsenev NK, Valiev RZ, Ma Y, Langdon TG (1993) An investigation of ductility and microstructural evolution in an Al-3% Mg alloy with submicron grain size, J Mater Res 8:2810-2818.
30. Stepanov ND, Yurchenko NYu, Tikhonovsky MA, Salishchev GA (2016) Effect of carbon content and annealing on structure and hardness of the CoCrFeNiMn-based high entropy alloys, J Alloy Compd 687:59-71.
31. Stepanov ND, Shaysultanov DG, Chernichenko RS, Yurchenko NYu, Zherebtsov SV, Tikhonovsky MA, Salishchev GA (2017) Effect of thermomechanical processing on microstructure and mechanical properties of the carbon-containing CoCrFeNiMn high entropy alloy, J Alloys Compd 693:394-405.
32. Laplanche G, Kostka A, Horst OM, Eggeler G, George EP (2016) Microstructure evolution and critical stress for twinning in the CrMnFeCoNi high-entropy alloy, Acta Mater 118:152-163.
33. Tabachnikova ED, Podolskiy AV, Laktionova MO, Bereznaia NA, Tikhonovsky MA, Tortika AS (2017) Mechanical properties of the $CoCrFeNiMnV_x$ high entropy alloys in temperature range 4.2-300 K, J. Alloys Comp. 698:501-509.
34. Podolskiy AV, Mangler C, Schafler E, Tabachnikova ED, Zehetbauer MJ (2013) Microstructure and mechanical properties of high purity nanostructured titanium processed by high pressure torsion at temperatures 300 and 77 K, J Mater Sci 48:4689-4697.
35. Lu K, Lu L, Suresh S (2009) Strengthening materials by engineering coherent internal boundaries at the nanoscale, Science 324:349-352.

36. Tsai CW, Chen YL, Tsai MH, Yeh JW, Shun TT, Chen SK (2009) Deformation and annealing behaviors of high-entropy alloy Al0.5CoCrCuFeNi, J Alloys Compd 486:427-435.
37. Zhang F, Zhang C, Chen SL, Zhu J, Cao WS, Kattner UR (2014) An understanding of high entropy alloys from phase diagram calculations, CALPHAD 451:1-10.
38. Otto F, Dlouhý A, Pradeep KG, Kuběnová M, Raabe D, Eggeler G, George EP (2016) Decomposition of the single-phase high-entropy alloy CrMnFeCoNi after prolonged anneals at intermediate temperatures, Acta Mater 112:40-52.
39. Pickering EJ, Muñoz-Moreno R, Stone HJ, Jones NG (2016) Precipitation in the equiatomic high-entropy alloy CrMnFeCoNi, Scr Mater 113:106-109.
40. Liu WH, Wu Y, He JY, Nieh TG, Lu ZP (2013) Grain growth and the Hall-Petch relationship in a high-entropy FeCrNiCoMn alloy, Scr Mater 68:526-529.
41. Bhattacharjee PP, Sathiaraj GD, Zaid M, Gatti JR, Lee C, Tsai C-W, Yeh J-W (2014) Microstructure and texture evolution during annealing of equiatomic CoCrFeMnNi high-entropy alloy, J Alloys Compd 587:544-552.
42. Sathiaraj GD, Bhattacharjee PP (2015) Analysis of microstructure and microtexture during grain growth in low stacking fault energy equiatomic CoCrFeMnNi high entropy and Ni-60 wt.%Co alloys, J Alloys Compd 637:267-276.

Figure captions:

Fig. 1 Microstructures of an as-cast sample (a,b) and an initial annealed sample (before HPT processing) (c,d) of a $CrFe_2NiMnV_{0.25}C_{0.125}$ HEA at different magnifications.

Fig. 2 Values of the Vickers microhardness measured across disks for the $CrFe_2NiMnV_{0.25}C_{0.075}$ and $CrFe_2NiMnV_{0.25}C_{0.125}$ HEAs after HPT processing through 5 turns: the lower dashed lines show the initial hardness values in the initial annealed condition.

Fig. 3 X-ray diffraction of (a) $CrFe_2NiMnV_{0.25}C_{0.075}$ and (b) $CrFe_2NiMnV_{0.25}C_{0.125}$HEAs before (Annealed sample) and after HPT processing through 5 turns.

Fig. 4 (a) TEM image and corresponding SAED pattern of the $CrFe_2NiMnV_{0.25}C_{0.125}$ HEA after 5 turns of HPT processing and (b) a chromium carbide particle in the matrix.

Fig. 5 X-ray patterns of the $CrFe_2NiMnV_{0.25}C_{0.125}$ HEA (a) after initial annealing and (b) after HPT processing, together with the effects of annealing at 823 and 1273 K for 60 min.

Fig. 6 STEM image of the $CrFe_2NiMnV_{0.25}C_{0.125}$ HEA after PDA at 823 K for 60 min.

Table caption:

Table 1 Chemical composition of the $CrFe_2NiMnV_{0.25}C_{0.125}$ alloy and its constituents.

Table 2 Microhardness of the $CrFe_2NiMnV_{0.25}C_{0.125}$ HEA under different conditions.

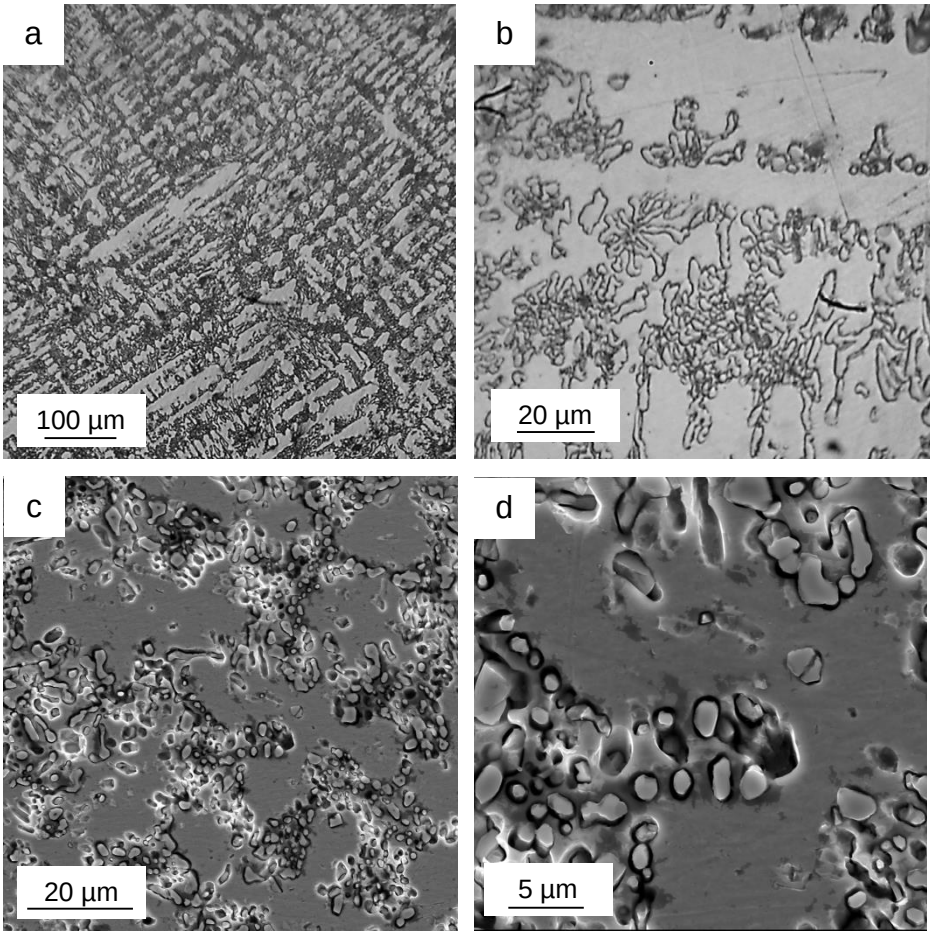

Fig. 1 Microstructures of an as-cast sample (a,b) and an initial annealed sample (before HPT processing) (c,d) of a $CrFe_2NiMnV_{0.25}C_{0.125}$ HEA at different magnifications.

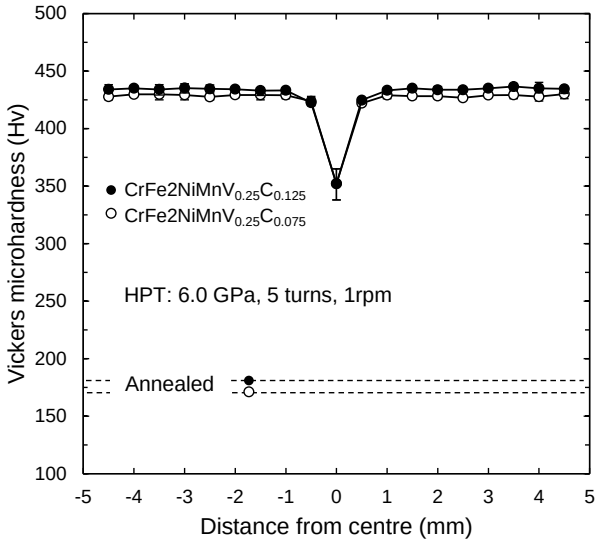

Fig. 2 Values of the Vickers microhardness measured across disks for the $CrFe_2NiMnV_{0.25}C_{0.075}$ and $CrFe_2NiMnV_{0.25}C_{0.125}$ HEAs after HPT processing through 5 turns: the lower dashed lines show the initial hardness values in the annealed condition.

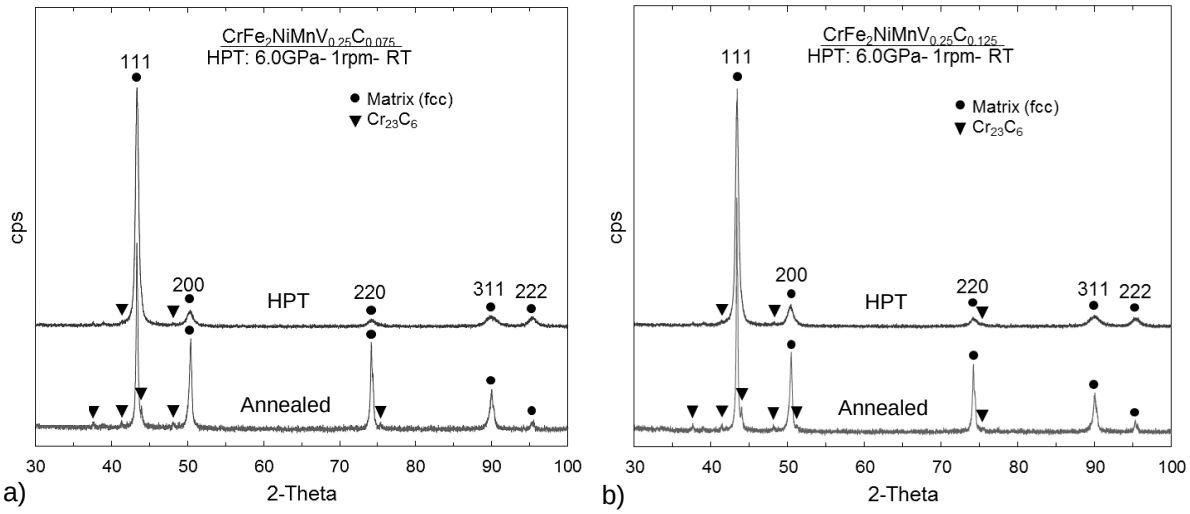

Fig. 3 X-ray diffraction of (a) $CrFe_2NiMnV_{0.25}C_{0.075}$ and (b) $CrFe_2NiMnV_{0.25}C_{0.125}$ HEAs before (Annealed sample) and after HPT processing through 5 turns.

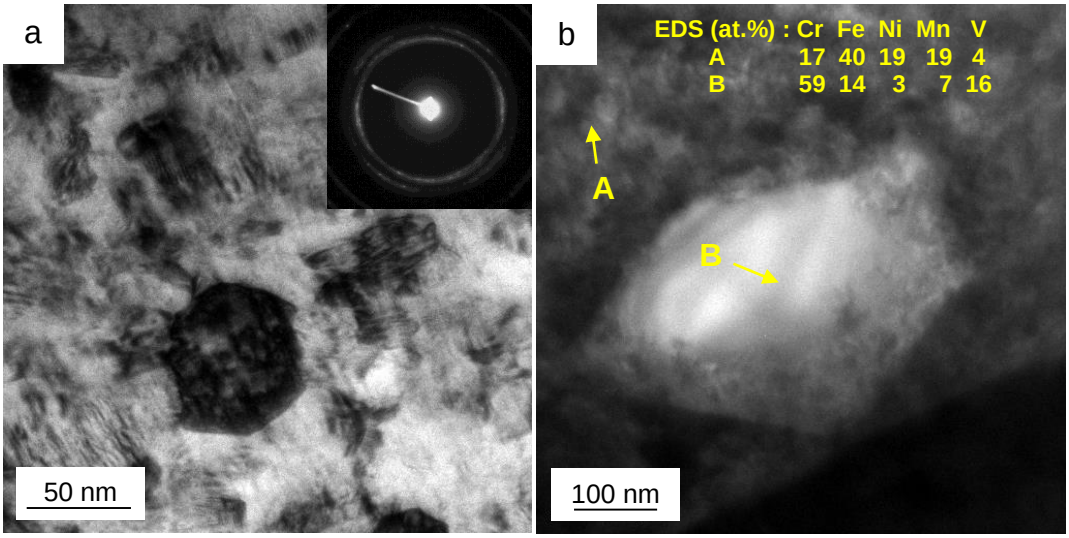

Fig. 4 (a) TEM image and corresponding SAED pattern of the $CrFe_2NiMnV_{0.25}C_{0.125}$ HEA after 5 turns HPT processing and (b) a chromium carbide particle in the matrix.

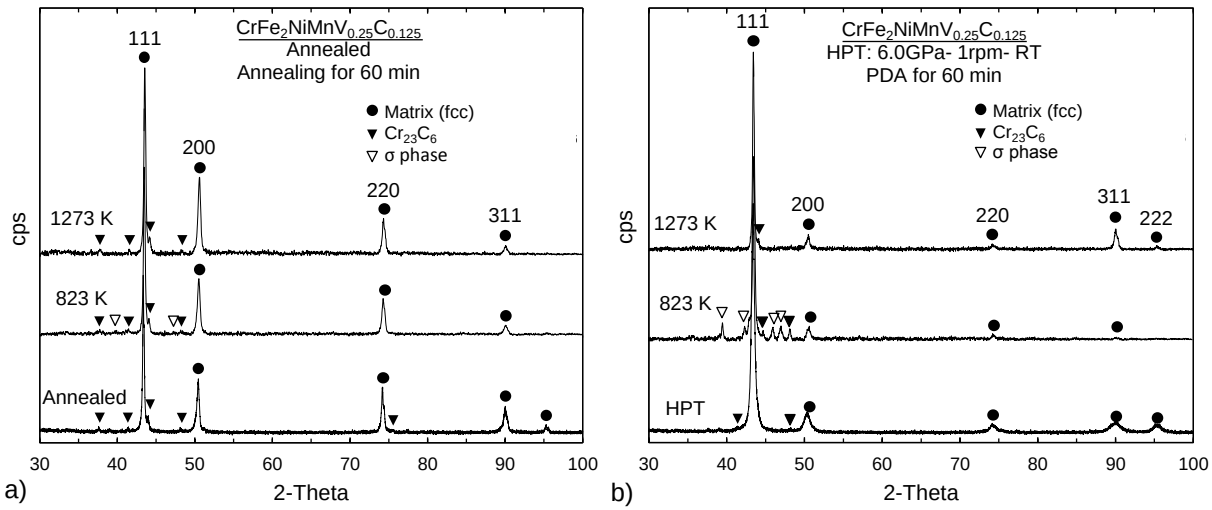

Fig. 5 X-ray patterns of the $CrFe_2NiMnV_{0.25}C_{0.125}$ HEA (a) after initial annealing and (b) after HPT processing, together with the effects of annealing at 823 and 1273 K for 60 min.

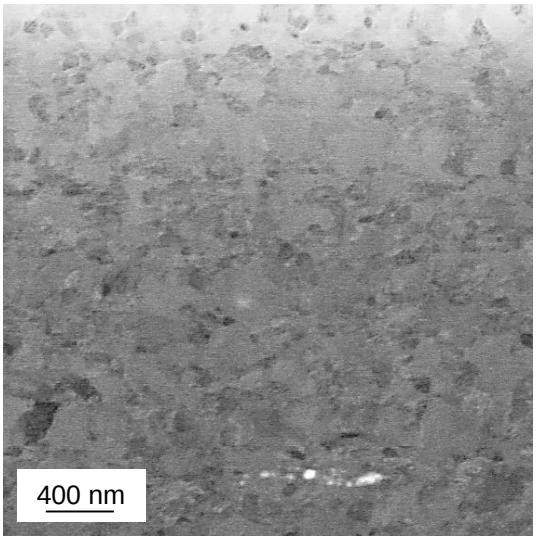

Fig. 6 STEM image of the $CrFe_2NiMnV_{0.25}C_{0.125}$ HEA after PDA at 823 K for 60 min.

Table 1 Chemical composition of the $CrFe_2NiMnV_{0.25}C_{0.125}$ alloy and its constituents.

Chemical composition	Elements (at %)					
	Cr	Fe	Ni	Mn	V	C
Nominal composition	18.6	37.2	18.6	18.6	4.7	2.3
Nominal composition*	19.0	38.2	19.0	19.0	4.8	-
Experimental composition*	21.3	37.0	17.8	18.4	5.5	-
Matrix composition*	15.2	40.7	20.7	19.9	3.5	-
Carbides composition*	54.8	15.5	3.9	11.1	14.7	-

*Without Carbon

Table 2 Microhardness of the $CrFe_2NiMnV_{0.25}C_{0.125}$ HEA under different conditions.

Condition	Hv
Initial coarse-grained	180±3
Annealed at 823 K for 60 min	190±4
Annealed at 1273 K for 60 min	180±2
HPT deformed: 6 GPa, 5 turns, 1rpm	435±2
HPT+annealing at 823 K for 60 min	555±3
HPT+annealing at 1273 K for 60 min	195±2